ADVANCED MATERIALS TECHNOLOGIES
www.advmattechnol.de

Flexible Janus Functional Film for Adaptive Thermal Camouflage

Yida Liu, Huaiyu Zuo, Wang Xi, Run Hu, and Xiaobing Luo*

With the increasing development of infrared (IR) detection technologies for both military and civil applications, IR anti-detection technologies, also known as thermal camouflage technologies, have attracted great attention in recent years. Decreasing the surface emissivity may be effective for high-temperature targets, but fails for adaptive thermal camouflage in dynamic scenes where the background temperature varies. In this work, we demonstrate a flexible Janus functional film (JFF) for adaptive thermal camouflage. The JFF consists of a low emissivity (low-ε) layer and a high heat capacity (high-C) layer. The low-ε layer can effectively suppress the IR radiation of the objects, thus reducing the temperature of the objects in IR camera, while the high-C layer can make similar thermal response as the background. According to different environmental conditions, different surfaces of JFF can be selected as camouflage surface to achieve static or dynamic thermal camouflage effect. What's more, the substrate materials of JFF (i.e., high-density polyethylene (HDPE), silica gel (SG)) enable the film with good flexibility and realize the encapsulation of the functional filler, thus improving its reliability of resisting water and oxygen. Such flexible JFF with high reliability, easy scalability, and low cost may hold great promise for broad applications in adaptive thermal camouflage.

1. Introduction

There have been many animals, such as cuttlefish, chameleon, and frog that have evolved with the capability of camouflage, which allows them to visually blend themselves into the background by changing their skin color, in order to achieve some biological purposes such as hunting, propagation, and hiding from predators.[1] Inspired by such biological camouflage capability, many researchers have been devoted to developing camouflage technologies to hide targets from detection in multi-physical fields, like in the visible band, infrared (IR) band, microwave band, and so on.[2–7] Among them, the camouflaging technologies in IR band are called as thermal camouflage, which aims at hiding targets from the IR detectors or cameras.[8,9] As we know, any objects with a temperature above absolute zero, of course, will spontaneously emit thermal radiation outwardly from anywhere and anytime, so it is more challenging to achieve thermal camouflage compared with the visible and microwave counterparts. Therefore, nowadays many military weapons are equipped with the IR cameras to assist locating targets through the anywhere and anytime thermal radiation, especially at night or dim scenarios. Thermal camouflage technologies aim at actively or passively adjusting the thermal radiation of the targets to approximate to that of its surrounding environment, so the object can be concealed into the background in the IR camera and thereby thermally camouflaged.

According to the Stefan–Boltzmann law, the detected thermal radiation energy (E) is proportional to the surface emissivity (ε) and the fourth power of thermodynamic temperature (T^4) of the target. Thus in general, the thermal camouflaging technologies can be categorized into two strategies. The first strategy is to tune the surface temperature, mainly through the emerging thermal metamaterials, which is effective due to the fourth power law ($E = \varepsilon\sigma T^4$) but challenging as temperature is hard to tune and maintain without additional heat or cold sources. Through thermal metamaterials with anisotropic thermal properties, the heat flow can be adjusted almost at will to achieve specific or even exotic temperature fields, thus yielding anti-detected[10,11] or "illusion" thermal signals.[12,13] However, such thermal metamaterials are usually hard to fabricate with naturally existing isotropic materials, limiting the practical applications of such metamaterials-based thermal camouflage technologies currently. In contrast, the second strategy which is based on surface emissivity engineering, has been the paradigm for the most thermal camouflaging technologies. In general, the targets have higher temperature than the ambient background, so the coatings or films with low emissivity can be effective to hide thermal signals and achieve thermal camouflage.[14,15] To achieve low emissivity engineering for thermal camouflage, people have proposed the photonic crystal-based multilayer film,[16,17] grating nanostructure,[18,19] nanoparticles-based materials,[20,21] functional textiles,[22] etc. By manipulating the distribution of electromagnetic fields through rational structure design, the photonic crystals can achieve superior low emissivity properties for thermal camouflage. However, such materials usually possess complex structures, leading to high processing cost, which impedes their

Y. Liu, H. Zuo, W. Xi, R. Hu, X. Luo
State Key Laboratory for Coal Combustion
School of Energy and Power Engineering
Huazhong University of Science and Technology
Wuhan 430074, China
E-mail: hurun@hust.edu.cn

The ORCID identification number(s) for the author(s) of this article can be found under https://doi.org/10.1002/admt.202100821.

DOI: 10.1002/admt.202100821

practical applications. The nanoparticles-based materials and functional textiles, on the other side, are relatively easier to fabricate, but the controllability on the emissivity is not that perfect, and the emissivity can only reach about 0.4.[20–22] Metal film, with merits like low emissivity and easy to fabricate, can meet the demand of thermal camouflage in general scene. Currently, the metal films have been used as radiative shielding layer in thermal camouflage net.[23] However, the metal films always suffer from the problem of low reliability, such as inflexible, easy oxidization, and corrosion.[24,25] On the other hand, the aforementioned structures with low emissivity can be merely used in static scene where the background temperature is lower than the thermal target. When the background temperature changes or is higher than the target temperature, thermal camouflage will become ineffective or even failure. To address this issue, the conventional emissivity engineering has been extended to dynamic emissivity manipulation, thus the thermal signal can match with the background in real time. Various approaches have been proposed to achieve adaptive thermal camouflage, such as electrical actuation of metasurface,[26] thermoelectric devices (TEDs)[27] and n-type quantum wells (QWs),[28] optical actuation of nanocrystal,[29] strain actuation of metamaterial emitter,[30] and so on. These adaptive devices are active and usually stimulated by external energy input, which undoubtedly increases the complexity and reduces their reliability and practicality.

To address these challenges, in this work, we propose a flexible Janus functional film (JFF) for adaptive thermal camouflage. The JFF is composed of substrate materials, including high-density polyethylene (HDPE) and silica gel (SG), enabling JFF with good flexibility, and the functional fillers, including micro-copper sheets (MCSs) and phase change microcapsules (PCMs). The front and back sides of JFF are characterized with low emissivity (low-ε) and high thermal capacity (high-C), respectively, which can satisfy the thermal camouflage functional requirements in general static scene with low temperature background and dynamic scene with changeable temperature background. In order to achieve both static thermal camouflage effect and mechanical flexibility, the content of functional fillers in low-ε layer of JFF is explored, and the optimal filler doping ratio is obtained with acceptable film flexibility. Then, by the accelerated life tests, we find that the JFF stands out with its merit of better corrosion resistance and reliability compared with traditional metal film owing to the packing structure of substrate material in JFF. Finally, we demonstrate the dynamic thermal camouflage effect of JFF in an imitated outdoor experiment. We believe flexible JFF with high reliability, easy scalability, and low cost can pave the way for adaptive thermal camouflage in practical applications.

2. Results and Discussions

2.1. Design for Flexible JFF

The adaptive flexible JFF consists of two functional layers, namely the low-ε layer and the high-C layer. As shown in **Figure 1**a, in the low-ε layer, the MCSs are uniformly distributed in the HDPE substrate. We choose MCSs as functional fillers owing to the low IR emissivity of copper and that the high concentration of the MCSs can form a lapping structure to achieve better IR thermal shielding effect, thus decreasing the IR emissivity of the layer. The HDPE featured by high IR transmissivity is used as the substrate material, enabling the low IR emissivity property of the MCSs un-affected. Then, the high-C layer is composed of PCMs and SG, where PCMs possess high thermal capacity owing to its large phase enthalpy, and the SG processes large intrinsic IR emissivity ($\varepsilon = 0.95$), synergistically enabling the high-C layer with high thermal capacity and high IR emissivity simultaneously. What's more, since all the substrate materials in JFF are flexible, JFF will also possess good flexibility as demonstrated experimentally later.

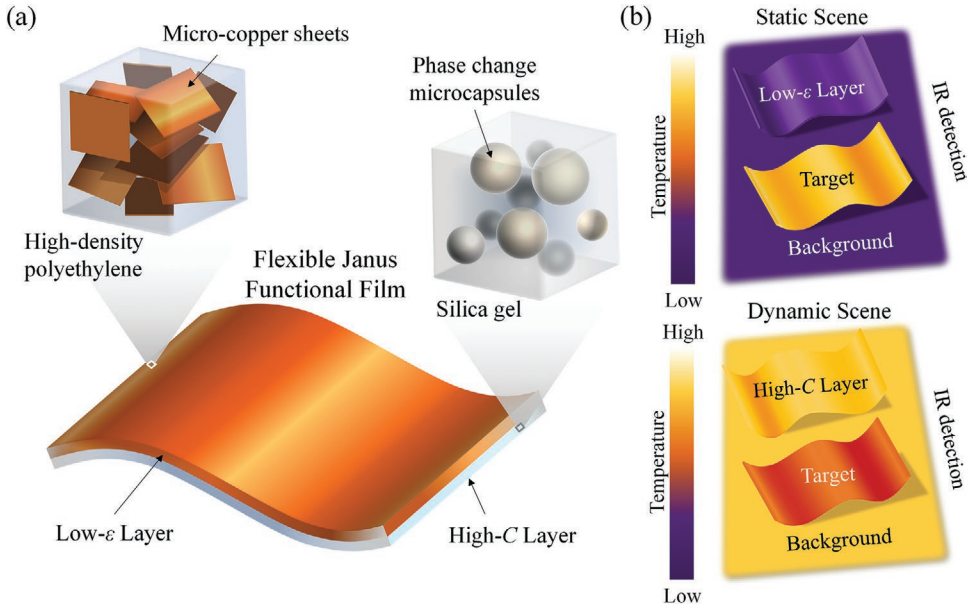

Figure 1. Structure and thermal camouflage performance of the flexible Janus functional film (JFF). a) Schematic diagram of the flexible JFF. b) Thermal camouflage performance of different layers of JFF working in different scenes.

Such JFF can meet the demand of thermal camouflage in different scenes. As shown in Figure 1b, when the low-ε layer is outward, the JFF can meet the thermal camouflage requirement for static scenes at low background temperature, which is similar to the working principle of most low-emissivity thermal camouflage materials.[16–18] For the dynamic scene where the temperature of the background is time-varying, the high-*C* layer will serve as the camouflage surface. The thermal properties of the high-*C* layer are similar to those of many backgrounds, such as large thermal capacity and high IR emissivity. Therefore, in the same circumstance, as the target and the background receive the same thermal stimulation, their response of temperature changes is almost the same, thus dynamic thermal camouflage effect can be achieved. Experimental demonstration of these two functions will be described in the following sections.

2.2. Thermal Camouflage in Static Scene

In the general static scene, the target objects like human body and electronic devices usually have higher temperature than the background, and thus low IR emissivity is demanded for thermal camouflage. In addition, the detection band of the IR camera is the same as the atmospheric window (3–5 µm, 8–14 µm), so only the IR emissivity in this dual-wavelength band is considered. Firstly, we investigate the influence of the mass fraction of MCSs on the IR emissivity of the low-ε layer in JFF. As shown in **Figure 2**a,b, the emissivity of low-ε layer decreases continuously with the mass fraction of MCSs increases, and when the mass fraction of MCSs reaches 90%, the emissivity can be suppressed around 0.2, which is lower than the most nanoparticle-based materials[20,21] and even some photonic crystal structure.[16] Note that, in the emissivity spectrum, there are two peaks at around 3.5 and 13.8 µm, which has adverse effect on the thermal camouflage. The peaks here are mainly caused by the substrate material HDPE. As shown in Figure 2c, the pure HDPE material has three high emissivity peaks in IR wavelengths, which originates from the chemical bond vibration, including asymmetric C–H stretching (3022 cm^{-1}), symmetric C–H stretching (2975 cm^{-1}), asymmetric CH_2 stretching (2891–2918 cm^{-1}), symmetric CH_2 stretching (2825–2849 cm^{-1}), asymmetric CH_2 bending (1472 cm^{-1}), CH_2 scissoring (1462 cm^{-1}), and CH_2 rocking (719–729 cm^{-1}).[31,32] Therefore, these unexpected emissivity peaks can be weakened by increasing the mass

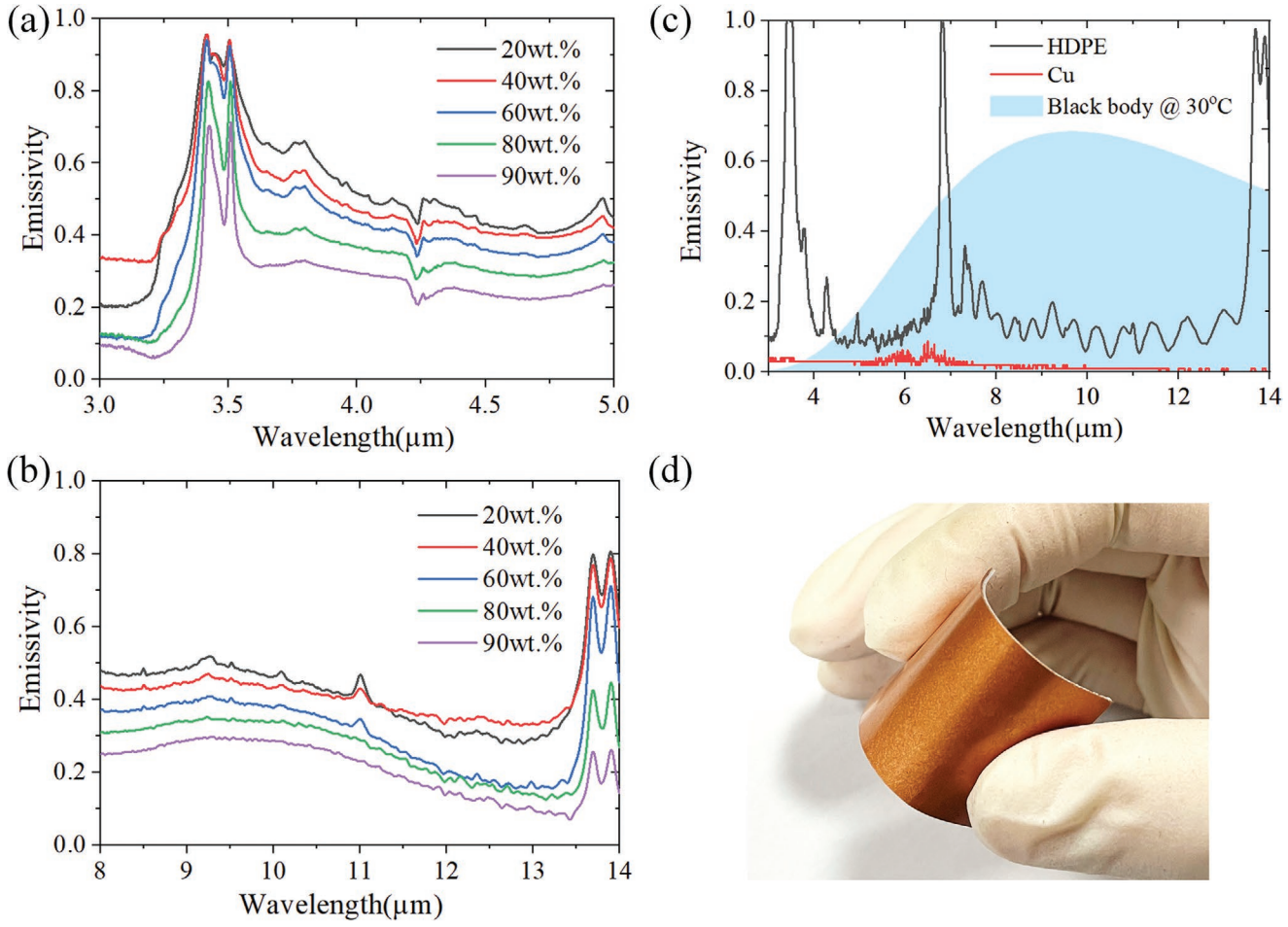

Figure 2. Measured emissivity spectrum of different films and photograph of Janus functional film (JFF). a,b) Emissivity spectrum of low-ε layer under various mass fraction of micro-copper sheets (MCSs) within 3–5 µm and 8–14 µm. c) Emissivity spectrum of pure high-density polyethylene (HDPE) film and Cu film within 3–14 µm and black body radiation spectrum at 30 °C. d) Photograph of flexible JFF with 90% mass fraction of MCSs.

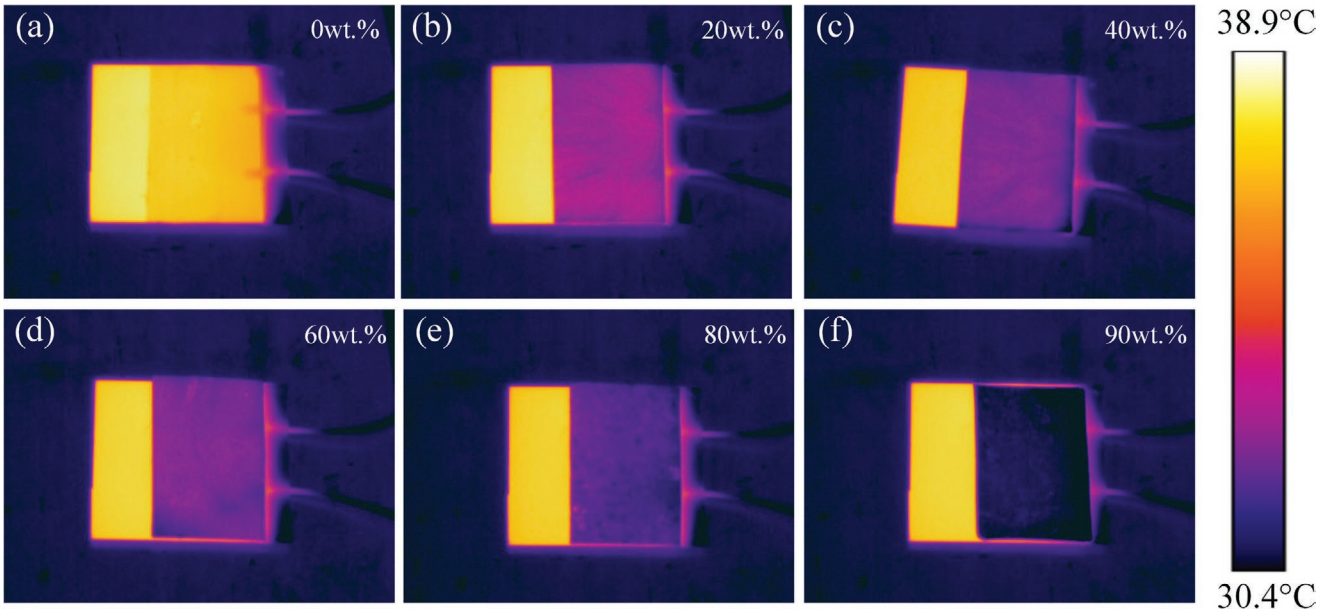

Figure 3. Thermal camouflage performance of Janus functional film (JFF) in static scene. a–f) Thermal images of JFF with micro-copper sheets (MCSs) mass fraction from 0% to 90%.

fraction of MCSs, but cannot be completely flattened. Nevertheless, PE is still regarded as a mainstream infrared-transparent functional material, owing to its excellent flexibility and wide-band high IR transmissivity.[22,33,34] As shown in Figure 2c, the black body radiation spectrum at 30 °C is illustrated with a light blue background. From the perspective of first detection band of 8–14μm, by increasing the mass fraction of MCSs, the intrinsic emissivity peak of HPDE at around 13.8 μm can suppressed below 0.3, thus, such emissivity peak would have no effect on the thermal camouflage performance. As for the second detection band of 3–5 μm, the black body radiation in this band is mainly concentrated in 4–5 μm, where the emissivity of JFF can be suppressed below 0.3, therefore the emissivity peak at 3.5 μm would have no significant effect on the thermal camouflage performance. What's more, though the thermal camouflage ability of JFF can be enhanced by increasing the mass fraction of MCSs, excessive content of MCSs will have a great impact on its flexibility. By trial and error, we find that when the mass fraction of MCSs exceeds 90%, JFF becomes brittle and is easy to break when bending. Therefore, 90% is taken as the optimal mass fraction of MCSs in low-ε layer, which enables the JFF with low IR emissivity and acceptable flexibility as shown in Figure 2d. It should be noted that though the intrinsic emissivity of the HDPE within the atmospheric window is low, the actual emissivity value is dependent on its thickness as the absorbed radiation will increase with the thickness of the HDPE film. The HDPE film we used in Figure 2b is only about 15 μm in thickness, while the total thickness of low-ε layer is above 50 μm. As for the low-ε layer with low MCSs concentration, the thickness of HDPE between MCSs and the layer surface may greatly exceed 15 μm, as shown in Figure S1b (Supporting Information). Besides, in the static camouflage experiment, when the radiation reaches the surface of JFF, it is first absorbed by the HDPE on the surface, then reflected by the MCSs inside and then re-absorbed by the HDPE. Therefore, as shown in Figure 2, the emissivity of pure HDPE film exhibits a lower emissivity ($\varepsilon = 0.2$) compared to that of low-ε with 20% mass fraction of MCSs ($\varepsilon = 0.4$).

In order to demonstrate the static thermal camouflage performance of JFF, we choose the heating plate (4×4 cm^2 in size) as the target to test the thermal camouflage effect of JFFs with different MCFs mass fraction. The heating plate is suspended over the background with two small pillars, so as to minimize the thermal conduction between the target and background. The heating plate is made of Al_2O_3 with its surface covered by black tape ($\varepsilon = 0.93$) which is used to increase the surface emissivity of the heating plate, because most targets possess high emissivity due to the paint decoration on their surface. For convenient observation and comparison, the heat plate is partly covered by the JFF, and in this static scene, the low-ε layer is used as the camouflage surface facing outwards. The background is made of aluminum with its surface hard-oxidized ($\varepsilon = 0.93$), whose emissivity is comparable with most of the backgrounds.[5] When the power source is turned on, the temperature of the heating plate begins to increase until reach an equilibrium at ≈38.9 °C, while the background temperature is about 30.4 °C. **Figure 3** depicts the thermal camouflage performance of JFF with MCSs mass fraction ranging from 0% to 90%. Apparently, the temperature of the JFF with MCSs mass fraction of 0% is almost the same as that of the heating plate due to the high IR transmissivity of HDPE (Figure 3a). With the increase of MCSs mass fraction, the IR emissivity of JFF decreases gradually, which leads to the improvement of its thermal camouflage effect. As the MCSs mass fraction reaches the optimal 90%, the temperature of JFF is almost identical to that of the background, and the covered part of the heating plate becomes invisible. As we can see from Figure 3, the low-ε layer can achieve a maximum pseudo temperature drop effect of about 9 °C. Therefore, the proposed JFF is generally suitable for heat camouflage when

the temperature of the environment and heat source does not exceed 10 °C.

The structure of low-ε layers with different mass fraction of MCSs is characterized by SEM, as shown in Figure S1 (Supporting Information). For the low-ε layer with relatively low mass fraction of MCSs (20%–60%), there is agglomeration of MCSs in the cross-section and many MCSs stays isolated in the matrix, resulting in a big interfacial thermal resistance. However, with the increase of the mass fraction (80%–90%), the volume of MCSs gradually expanded, which greatly improves their distribution uniformity and the MCSs begins to interconnect, thus reducing the interfacial thermal resistance and making the camouflage temperature fields more uniform, which also can be verified in Figure 3, the camouflage temperature field of JFF with high mass fraction of MCSs is more uniform than that of JFF with low MCSs mass fraction. In addition, since the low-ε layer is made by thermal pressing process, the MCSs can be distributed in parallel in the layer. In the low-ε layers with high mass fraction, the MCSs are distributed in parallel and kept interconnected, thus forming a structure like a multilayer shield inside the layer, which results in excellent thermal camouflage performance of the low-ε layers. In order to evaluate the mechanical properties of different samples, the uniaxial tensile test has also been carried out. As shown in Figure S2 (Supporting Information), since there is no extra bond between MCSs and HDPE, the mechanical properties of the film are inversely proportional to its thermal camouflage performance, which indicates that the JFFs with good camouflage effect are more suitable for some camouflage objects with relatively flat surface structure, while for objects with complex surface structure and high requirements for mechanical properties of the JFF, a certain thermal camouflage effect should be sacrificed to improve its mechanical properties. We have conducted shear strength tests on JFF with PCMs contents of 0% and 40% to investigate interfacial adhesion between the low-ε layer and high-C layer. The shear strength of the former is about 0.12 MPa while that of the latter is about 0.09 MPa. Increasing the content of phase change material has a certain effect on the interface adhesion of JFF, but it can still get a good adhesion effect, according to the experimental results.

Low IR emissivity is an indispensable property for static thermal camouflaging materials. However, in practical applications, the reliability of materials should be taken into consideration, especially in the outdoor environment. We have conducted an accelerated life test to demonstrate the good reliability of JFF compared with the Cu film which possesses superior low IR emissivity property (Figure 2c). The Cu film (**Figure 4**a) and JFF (Figure 4b) with same area are selected for the accelerated life test. The two films are placed into two water baths with same volume, respectively. The temperature of the water is controlled at 60 °C. After 7 days of accelerated life test, the two films are taken out for subsequent thermal camouflage performance test. As shown in Figure 4b, after the accelerated life test, a large amount of verdigris appears on the surface of the Cu film, which is caused by the chemical reaction of the copper with the carbon dioxide and water in the water bath. By contrast, the surface of JFF shows little changes as shown in Figure 4d. (The properties of the high-C layer in JFF do not change much either after the test, which is not shown here.) As shown in Figure 4e, we put the corroded Cu film and JFF on the lower and upper sides of the heating plate surface, the temperature of the uncorroded part of the Cu film is still close to that of the background, while the temperature of the verdigris is close to that of the heating plate owing to the high IR emissivity of the verdigris, which deteriorates the static thermal camouflage performance. However, the thermal camouflage performance of JFF film is consistent with the above megascopic results and has not been affected. Although metal films always possess excellent low IR emissivity property, most of the metal materials are chemically active. Therefore, in practical application, there are still many reliability problems existing, such as oxidation and corrosion. In the JFF, MCSs are insulated from the external environment by the packaging of HPDE. Despite the low IR emissivity property of the composite material is not comparable to that of the pure metals, this strategy successfully solves the problem of corrosion and oxidation while possessing good thermal camouflage performance simultaneously.

2.3. Thermal Camouflage in Dynamic Scene

When the target is exposed to the outdoor scenario, its temperature will be affected by the external environment, such as solar illumination variation in the daytime and nighttime. In this kind of dynamic scene, the change of solar illumination will lead to the release or storage of heat by the environment and target. In this way, the difference of thermal properties between the object and the environment will result in great

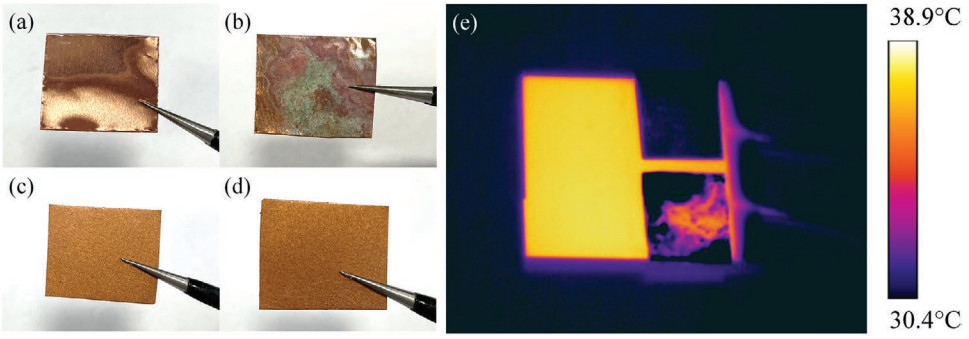

Figure 4. Demonstration of the high reliability of Janus functional film (JFF). Photograph of a) Cu film and c) JFF before accelerated life test, and b) Cu film and d) JFF after accelerated life test. e) Thermal camouflage performance of the Cu film and JFF after accelerated life test.

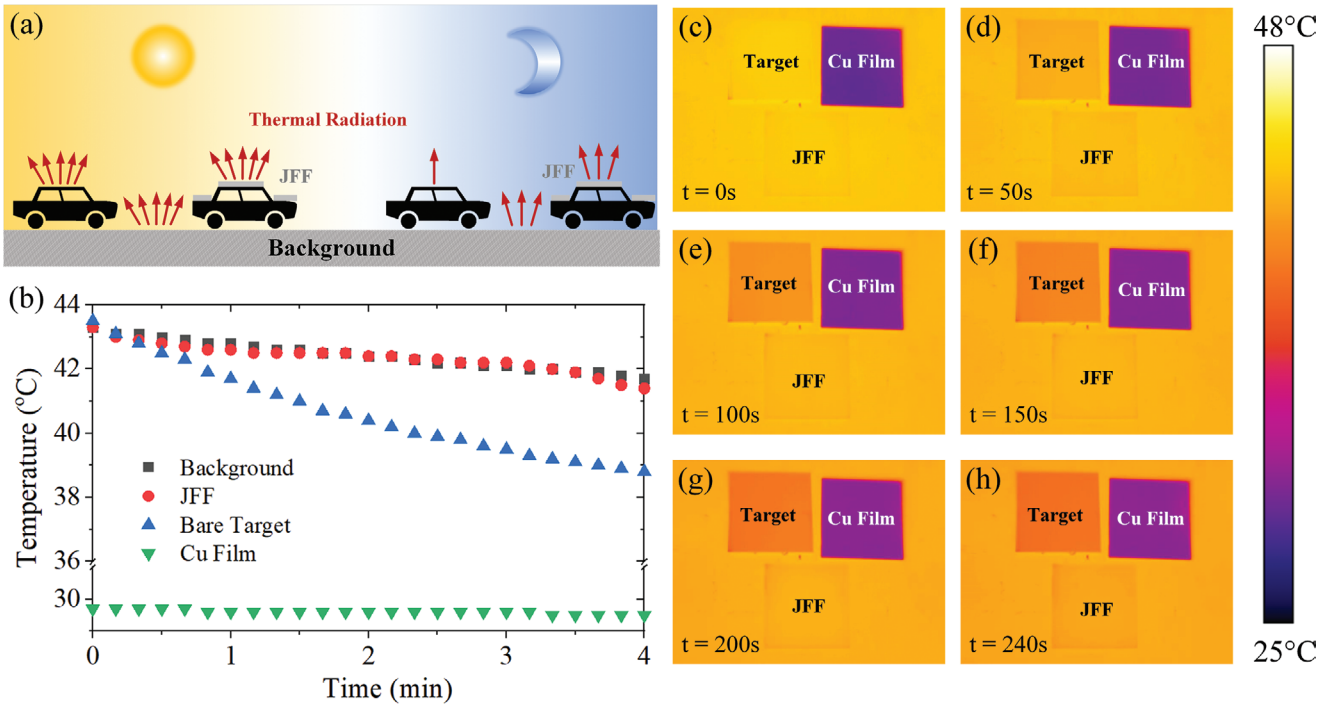

Figure 5. Thermal camouflage performance of Janus functional film (JFF) in dynamic scene. a) Schematic of dynamic thermal camouflage mechanism of JFF. b) Temperature-time plots of bare target, JFF, Cu film, and background in infrared (IR) camera. c–h) IR images of bare target, JFF, Cu film and background at different times.

differences between their thermal radiation, thus the target can be easily detected by the IR camera. To address this issue, the thermal camouflage film should be designed to possess the similar thermal properties with the background environments, such as high IR emissivity and large thermal capacity. Therefore, it is understandable that the typical thermal camouflage films with ultra-low IR emissivity are no longer suitable for thermal camouflage in this dynamic scene. The high-*C* layer in JFF is designed as the camouflage surface for dynamic thermal camouflage. In this layer SG is used as the substrate material, which enables the JFF with high IR emissivity of approximately 0.95, comparable with most of the backgrounds.[5] What's more, the PCMs are used as the functional fillers to enhance the thermal capacity of JFF for the phase-change materials can exhibit large thermal capacity near the phase-transition temperature by storing or releasing thermal energy as latent heat.

Figure 5a illustrates the working principles of JFF in dynamic scene. In the daytime with sunlight illumination, the temperature of the target and the background will increase continually until reach an equilibrium owing to the absorption of solar radiation and dissipation via convection and conduction. Then, as the sunlight illumination decreases or disappears (e.g., cloudy or nighttime), the temperature of the target will decrease rapidly by nature convection, resulting in a steep decline of its IR radiation, whereas the temperature of the background and JFF decrease gradually owing to their relatively high thermal capacity. The PCMs in the high-*C* layer of JFF can effectively inhibit the temperature drop through the release of latent heat during the phase-transition process, so as to delay the decrease rate of thermal radiation and thus match with the background. Therefore, the temperature and radiation of JFF can always be consistent with the background in this dynamic scene. We conduct an imitated outdoor experiment to demonstrate the dynamic thermal camouflage performance of JFF. Three identical ceramic plates were selected as targets suspended in the background, two of which are covered with the same area Cu film and JFF, respectively. The background here is consistent with that of the static experiment (aluminum with surface hard-oxidized). In this dynamic scene, the high-*C* layer is used as camouflage surface facing outwards. Firstly, the three targets and background are heated up to approximately 44 °C by radiant heater, which is regarded as the equilibrium state of the system under outdoor sunlight illumination. The phase-transition temperature of PCMs in JFF is 42 °C, which is approximate to the equilibrium temperature for achieving better dynamic thermal camouflage performance. It should be noted that the PCMs with different phase transition temperature can be used in JFF according to its working environment. Then the radiant heater is turned off and system is cooled down through natural convection dissipation, during which the temperature of the system variation is captured by the IR camera. Figure 5b records the temperature of the targets and background at different times. It is apparent that the temperature of the bare target drops rapidly over time, and the temperature difference between the target and background has exceeded 3 °C at 4 min, while the temperature of JFF decreases gradually and always approaches to the temperature of the background, and the temperature difference is less than 0.3 °C. As for the Cu film, owing to its ultra-low IR emissivity, its real surface temperature variation has little effect on the IR radiation, so the surface temperature

variation of the Cu film in the IR camera is not obvious, which is maintained around 30 °C. To make the dynamic camouflage more intuitive, we have selected some IR images at specific moments shown in Figure 5c–h. At the initial time, the temperature of the bare target and the JFF is consistent with that of the background, whereas the Cu film is exposed to the background due to its extremely low surface temperature. Then, at t = 50—240 s, the bare target begins to appear in the IR images while the JFF stays vanished in the background, demonstrating excellent dynamic thermal camouflage performance.

To further explore the adaptability of JFF in different environments, we have performed a simplified heat transfer calculation to find the relationship between material parameters of high-*C* layer and background as:

$$\rho_b c V (T_h - T_l) = h A_b (T_m - T_a) \tau \quad (1)$$

$$A_J \rho_J \varphi d H_p = h A_J (T_m - T_a) \tau \quad (2)$$

where ρ_b and ρ_J denote the density of the background and high-*C* layer, A_b and A_J denote the cooling surface area of background and high-*C* layer, c denotes the specific heat of the background, V is the volume of the background, T_m is phase-transition temperature of PCMs, $T_h = T_m + 0.5$ and $T_l = T_m - 0.5$ represent the upper bound and lower bound of the temperature of background for the duration of dynamic thermal camouflage, (here we define the time when the high-C layer and the background temperature do not exceed 0.5 °C as the effective time of dynamic thermal camouflage.) T_a is the ambient temperature, h is the convective heat transfer coefficient, d is the thickness of high-*C* layer, φ is the mass fraction of PCMs in high-*C* layer, H_p is the phase enthalpy of PCMs and τ is the duration of dynamic thermal camouflage. By combining the above two equations, the control equation of material parameters of high-*C* layer can be obtained:

$$\rho_J \varphi H_p d = \frac{c\rho_b (T_h - T_l)}{A_b} = \frac{c\rho_b V}{A_b} \quad (3)$$

As shown in Equation (3), the material parameters of PCMs and the thickness of the high-*C* layer are strongly correlated with the background environment. According to different background environmental parameters, the material parameters of the high-*C* layer need to be adjusted relatively. According to the requirements of different scenes, the simplified heat transfer calculation can be carried out first to determine the required functional parameters which, then, should be taken as the targets to guide the PCMs selection and configuration in high-*C* layer, so that the corresponding JFFs can be manufactured according to the requirements of different scenes. What's more, owing to the limitation of substrate material, the JFF cannot be used in excessively high temperature conditions for the HDPE will soften under high temperature environments, which will cause structural destruction and failure. The proposed JFF is mainly used for dynamic thermal camouflage in outdoor environment where the temperature of the background is typically ranging from 20 °C to 60 °C.

3. Conclusion

In conclusion, we proposed a flexible JFF for adaptive thermal camouflage, which is composed of a low-ε layer (MCSs/HDPE) and a high-*C* layer (PCMs/SG). In the static scene, the low-ε layer can be used as the camouflage surface, which possesses relative low IR emissivity. It has been demonstrated by the experiment that as the mass fraction of MCSs increases in low-ε layer, its IR emissivity will decrease continuously, leading to the improvement of static thermal camouflage performance. On the premise of considering flexibility of the film, the optima mass fraction of MCSs is selected as 90%. What's more, compared to the common metal film with superior low IR emissivity property, the reliability of the JFF of resisting water and oxygen has been greatly improved, which enhances its feasibility in practical applications. In the dynamic scene, the camouflage surface will be switched to high-*C* layer, which possesses high IR emissivity and large thermal capacity, similar to most of the backgrounds. Then, in an imitated outdoor experiment, when the external heater is turned off, the temperature difference between the JFF and background temperature is always less than 0.3 °C, while the temperature difference between the exposed target and background temperature is up to 3 °C, which proves the good dynamic thermal camouflage performance of JFF. This flexible JFF with high reliability and low cost can also be easily to scale up, and may open the avenue for adaptive thermal camouflage in practical applications.

4. Experimental Section

Materials: HDPE was purchased from Sigma Aldrich. MCSs were purchased from Xuzhou Chuangjie New Material Technology Co., Ltd. PCMs were purchased from Shanghai Rushang New Energy Technology Co., Ltd. SG was purchased from Dow Corning Company. Toluene was purchased from Shanghai Hushi Company and used as received, which was used for the subsequent fabrication process.

Fabrication of Flexible Janus Functional Film: Taking the fabrication of JFF with MCSs mass fraction of 90% in low-ε layer as an example, the MCSs with an average diameter of 20 µm were mixed with HDPE at a weight ratio of MCS:HDPE = 9:1 in toluene. The volume of toluene is 12 times the weight of the HDPE. The mixture was then put on a heating magnetic stirrer at the temperature of 150 °C and magnetic ball rotates at the speed of 350 rmp for 1 h. After the HDPE was completely dissolved, the mixture was poured out and scraped into a film which was then dried in an oven for 3 h at 50 °C. Next, the film was smashed into powders and dried in oven for another 2 h at 50 °C. The composite powders were melt-pressed in a vacuum thermal press at temperature of 160 °C and a pressure of 2.5 MPa to obtain the composite film (i.e., the low-ε layer in JFF). Then the high-*C* layer was going to made. The PCMs (melt point 42 °C) were mixed with SG at a weight ratio of PCM:SG = 2:3, excessive PCM content would make SG uncurable. The mixture was then stirred for 10 min to ensure that the particles were dispersed uniformly. Bubbles introduced by stir were then removed by repeat cycles of vacuum. The mixed gel was coated onto the surface of the low-ε layer by doctor blading. After the mixed gel is cured by the curing procedure in vacuum oven at 80 °C for 5 h, the JFFs were obtained.

Characterization on Morphology and Mechanical Properties: The morphology of the low-ε layers was characterized by a scanning electron microscope (Hitachi S4800) with an acceleration voltage of 5 kV. The tensile stress–strain curves were recorded by using a Universal testing machine.

Characterization on Thermal Camouflage: The IR reflectivity (ρ) of the low-ε layer was measured by a FTIR (Nicolet iS50R) equipped with a gold

integrating sphere. The transmissivity of the low-ε layer is measured to be negligible, so its absorptivity (α) can be calculated as 1–ρ. According to Kirchhoff's law, the emissivity can be obtained as $\varepsilon = \alpha$. The thermal images were taken by an FLIR SC620 IR thermal imager. It should be mentioned that all the thermal images were captured in an open environment with natural thermal radiation and thermal convection.

Supporting Information

Supporting Information is available from the Wiley Online Library or from the author.

Acknowledgements

Y.L. and H.Z. contribute equally to this work. This work was supported by National Natural Science Foundation of China (52076087), and Wuhan City Science and Technology Program (2020010601012197).

Conflict of Interest

The authors declare no conflict of interest.

Data Availability Statement

The data that support the findings of this study are available from the corresponding author upon reasonable request.

Keywords

adaptive thermal camouflage, flexible functional film, infrared technology, phase-change materials

Received: July 6, 2021
Revised: September 16, 2021
Published online:

[1] R. Hanlon, *Curr. Biol.* **2007**, *17*, R400.
[2] S. A. Morin, R. F. Shepherd, S. W. Kwok, A. A. Stokes, A. Nemiroski, G. M. Whitesides, *Science* **2012**, *337*, 828.
[3] G. Wang, X. Chen, S. Liu, C. Wong, S. Chu, *ACS Nano* **2016**, *10*, 1788.
[4] H. Chen, B. Zheng, L. Shen, H. Wang, X. Zhang, N. I. Zheludev, B. Zhang, *Nat. Commun.* **2013**, *4*, 2652.
[5] J. Lyu, Z. Liu, X. Wu, G. Li, D. Fang, X. Zhang, *ACS Nano* **2019**, *13*, 11392.
[6] Y. Li, X. Bai, T. Yang, H. Luo, C.-W. Qiu, *Nat. Commun.* **2018**, *9*, 273.
[7] C. Yu, Y. Li, X. Zhang, X. Huang, V. Malyarchuk, S. Wang, Y. Shi, L. Gao, Y. Su, Y. Zhang, H. Xu, R. T. Hanlon, Y. Huang, J. A. Rogers, *Proc. Natl. Acad. Sci. USA* **2014**, *111*, 12998.
[8] R. Hu, W. Xi, Y. Liu, K. Tang, J. Song, X. Luo, J. Wu, C.-W. Qiu, *Mater. Today* **2021**, *45*, 120.
[9] J. Song, S. Huang, Y. Ma, Q. Cheng, R. Hu, X. Luo, *Opt. Express* **2020**, *28*, 875.
[10] T. Han, X. Bai, D. Gao, J. T. L. Thong, B. Li, C.-W. Qiu, *Phys. Rev. Lett.* **2014**, *112*, 054302.
[11] H. Xu, X. Shi, F. Gao, H. Sun, B. Zhang, *Phys. Rev. Lett.* **2014**, *112*, 054301.
[12] R. Hu, S. Zhou, Y. Li, D.-Y. Lei, X. Luo, C.-W. Qiu, *dv. Mater.* **2018**, *30*, 1707237.
[13] R. Hu, S. Huang, M. Wang, X. Luo, J. Shiomi, C.-W. Qiu, *Adv. Mater.* **2019**, *31*, 1807849.
[14] K. K. Gupta, A. Nishkam, N. Kasturiya, *J. Ind. Text.* **2001**, *31*, 27.
[15] H. Zhang, J. C. Zhang, *J. Text. Inst.* **2008**, *99*, 83.
[16] L. Peng, D. Liu, H. Cheng, S. Zhou, M. Zu, *Adv. Opt. Mater.* **2018**, *6*, 1801006.
[17] H. Zhu, Q. Li, C. Zheng, Y. Hong, Z. Xu, H. Wang, W. Shen, S. Kaur, P. Ghosh, M. Qiu, *Light: Sci. Appl.* **2020**, *9*, 60.
[18] M. Pan, Y. Huang, Q. Li, H. Luo, H. Zhu, S. Kaur, M. Qiu, *Nano Energy* **2020**, *69*, 104449.
[19] E. Buhara, A. Ghobadi, B. Khalichi, H. Kocer, E. Ozbay, *J. Phys. D: Appl. Phys.* **2021**, *54*, 265105.
[20] J. Mandal, S. Du, M. Dontigny, K. Zaghib, N. Yu, Y. Yang, *Adv. Funct. Mater.* **2018**, *28*, 1802180.
[21] H. Ji, D. Liu, C. Zhang, H. Cheng, *Sol. Energy Mater. Sol. Cells* **2018**, *176*, 1.
[22] M. S. Ergoktas, G. Bakan, P. Steiner, C. Bartlam, Y. Malevich, E. O. Yenigun, G. He, N. Karim, P. Cataldi, M. A. Bissett, I. A. Kinloch, K. S. Novoselov, C. Kocabas, *Nano Lett.* **2020**, *20*, 5346.
[23] G. Li, D. Liu, Y. Wang, H. Chen, Z. Luo, *Infrared Technol* **2019**, *41*, 495.
[24] Ž. Z. Tasić, M. B. P. Mihajlović, M. B. Radovanović, M. M. Antonijević, *Chem. Pap.* **2019**, *73*, 2103.
[25] L. Nguyen, T. Hashimoto, D. N. Zakharov, E. A. Stach, A. P. Rooney, B. Berkels, G. E. Thompson, S. J. Haigh, T. L. Burnett, *ACS Appl. Mater. Interfaces* **2018**, *10*, 2230.
[26] Y. Liu, J. Song, W. Zhao, X. Ren, Q. Cheng, X. Luo, N. X. Fang, R. Hu, *Nanophotonics* **2020**, *9*, 855.
[27] S. Hong, S. Shin, R. Chen, *Adv. Funct. Mater.* **2020**, *30*, 1909788.
[28] T. Inoue, M. D. Zoysa, T. Asano, S. Noda, *Nat. Mater.* **2014**, *13*, 928.
[29] Z. J. Coppens, J. G. Valentine, *Adv. Mater.* **2017**, *29*, 1701275.
[30] X. Liu, W. J. Padilla, *Adv. Mater.* **2016**, *28*, 871.
[31] D. Li, X. Liu, W. Li, Z. Lin, B. Zhu, Z. Li, J. Li, B. Li, S. Fan, J. Xie, J. Zhu, *Nat. Nanotechnol.* **2021**, *16*, 153.
[32] J. Charles, G. R. Ramkumaar, *Asian J. Chem.* **2009**, *24*, 4477.
[33] L. Cai, A. Y. Song, W. Li, P.-C. Hsu, D. Lin, P. B. Catrysse, Y. Liu, Y. Peng, J. Chen, H. Wang, J. Xu, A. Yang, S. Fan, Y. Cui, *Adv. Mater.* **2018**, *30*, 1802152.
[34] R. Hu, Y. Liu, S. Shin, S. Huang, X. Ren, W. Shu, J. Cheng, G. Tao, W. Xu, R. Chen, X. Luo, *Adv. Energy Mater.* **2020**, *10*, 1903921.